

Automated improvement of stickleback reference genome assemblies with Lep-Anchor software

Mikko Kivikoski^{†1} | Pasi Rastas^{†2} | Ari Löytynoja² | Juha Merilä^{1,3}

¹Organismal and Evolutionary Biology Research Programme, Faculty of Biological and Environmental Sciences, FI-00014 University of Helsinki, Finland

²Institute of Biotechnology, FI-00014 University of Helsinki, Finland

³Division of Ecology and Biodiversity, Kadoorie Building, The University of Hong Kong, Pokfulam Road, Hong Kong, SAR

Correspondence

Mikko Kivikoski, Faculty of Biological and Environmental Sciences, FI-00014 University of Helsinki, Finland. Email: mikko.kivikoski@helsinki.fi

Ari Löytynoja, Institute of Biotechnology, FI-00014 University of Helsinki, Finland. Email: ari.loytynoja@helsinki.fi

[†]These authors contributed equally to this work.

Summary

We describe an integrative approach to improve contiguity and haplody of a reference genome assembly and demonstrate its impact with practical examples. With two novel features of Lep-Anchor software and a combination of dense linkage maps, overlap detection and bridging long reads we generated an improved assembly of the nine-spined stickleback (*Pungitius pungitius*) reference genome. We were able to remove a significant number of haplotypic contigs, detect more genetic variation and improve the contiguity of the genome, especially that of X chromosome. However, improved scaffolding cannot correct for mosaicism of erroneously assembled contigs, demonstrated by a de novo assembly of a 1.7 Mbp inversion. Qualitatively similar gains were obtained with the genome of three-spined stickleback (*Gasterosteus aculeatus*). Since the utility of genome-wide sequencing data in biological research depends heavily on the quality of the reference genome, the improved and fully automated approach described here should be helpful in refining reference genome assemblies.

KEYWORDS:

Genome assembly, Haplotype, Mosaicism, Stickleback, *Pungitius*, *Gasterosteus*

1 INTRODUCTION

2 Great deal of present-day research in biology is based on genomic data
3 that are processed and analyzed in the context of a linear reference
4 genome. Typical examples of this are whole-genome sequencing studies
5 where sequencing reads are mapped to the reference genome and the
6 characteristics of interest are derived from local dissimilarities and
7 statistics based on the alignments (Korneliussen, Albrechtsen, & Nielsen
8 2014; Schraiber & Akey 2015). Reliability of those characteristics and
9 the conclusions drawn from them depend not only on the quality of
10 the sequencing data but also on the quality of the reference genome.
11 Assembling and evaluating the quality of reference genomes is not easy
12 (Baker 2012; Church et al. 2011; Meltz Steinberg et al. 2017; Rice
13 & Green 2019). The profound problem is that the physical connectivity
14 is lost during sequencing and recovering that in the assembly stage is
15 notoriously difficult. To this end, high-quality linkage maps are valuable
16 and allow inferring the physical order and orientation of the assembled
17 contigs (Pengelly & Collins 2019; Rastas 2020; Stemple 2013).

18 Although a linear reference genome is ill-suited for describing many
19 structural variations, most genome analysis methods assume the reference
20 genome to contain each genomic region only once. The continuous
21 development of the human reference genome (Schneider et al. 2017;
22 Sherman & Salzberg 2020) has shown that creating a linear haploid
23 reference genome for a diploid species is a non-trivial task. Reaching
24 this ideal can be especially challenging in organisms where the genetic
25 variation cannot be reduced in controlled inbreeding designs, and most
26 reference genomes are likely based on reference individuals carrying
27 long alternative haplotypes (Chin et al. 2016; Howe et al. 2013; Stemple
28 2013). Presence of homologous haplotypes, that is, differing copies
29 of the same genomic region inherited from the two parents, is against
30 the assumptions of the linear reference genome and affects for instance
31 the read mapping. If reads from distinct haplotypes map to different
32 copies of the same region, single nucleotide variants (SNPs) separating
33 the haplotypes cannot be detected and variation is underestimated. This
34 affects various statistics in population genomics, and may lead to wrong
35 conclusions in many different contexts, including estimation of substitution
36 rate (Kong et al. 2012), inbreeding (Ceballos, Joshi, Clark, Ramsay,
37 & Wilson 2018) or population history (Roux et al. 2016).

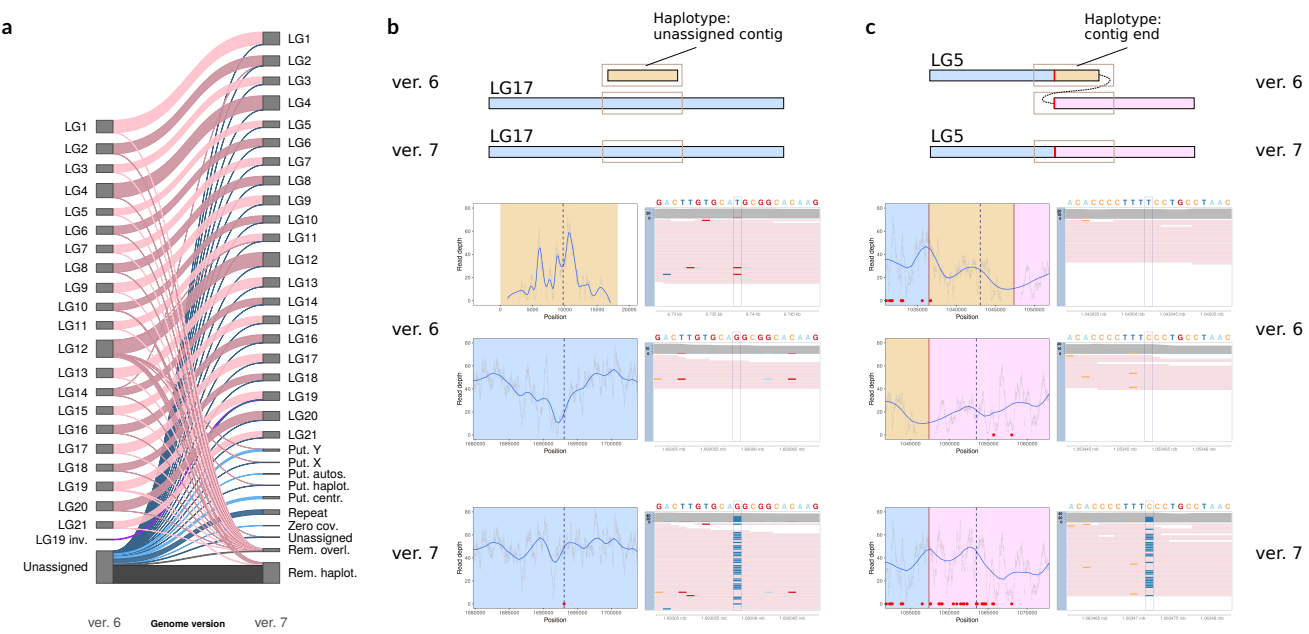


FIGURE 1 Summary of the changes between ver. 6 and ver. 7 of the nine-spined stickleback reference genome and examples of removed haplotypes. (a) Diagonal lines indicate changes in contig placement between different linkage groups (LGs) with band widths proportional to the length of the contigs with the corresponding change. Unassigned contigs in ver. 7 were grouped into putative classes according to their sequencing coverage and repeat content (see methods). (b, c) A schematic illustration of regions in the two assemblies is shown on top and the data for the highlighted areas (boxes) in the panels below. On the left, blue curves show the smoothed read depth and the dashed lines indicate a SNP position, boxed in the right panel. On the right, the reference sequence is shown on top and the pink bars indicate mapped reads, mismatches shown with matching colors. (b) A short, unassigned contig (orange) was identified as a haplotype within a contig (blue) in LG17. After its removal (ver. 7, bottom), the read depth is more even and a new SNP (red dot) is identified. (c) A region (orange) was duplicated in the ends of neighboring contigs (blue, pink) in LG5. After its removal (ver. 7, bottom; cut site in red), the read depth is more even and several new SNPs are identified.

38 Lep-Anchor software (Rastas 2020) can improve assembly and scaf-
 39 folding of even high-quality reference genomes with joint use of linkage
 40 map based genome anchoring, pairwise contig alignment and long-
 41 read sequencing data. Performance and utility of Lep-Anchor were
 42 demonstrated in its original publication (Rastas 2020) with empirical
 43 and simulated data sets and gains in assembly quality were reported
 44 even with relatively small data sets. Here, we have a closer look on
 45 the actual changes and assess their impact on typical genome anal-
 46 yses. Starting from an existing high-quality contig assembly, original
 47 PacBio reads and ultra-dense linkage maps for the nine-spined stick-
 48 leback (*Pungitius pungitius*), we were able to generate a significantly
 49 improved reference genome (ver. 7) using largely automated methods.
 50 When evaluating the differences to the published version of the refer-
 51 ence genome (ver. 6; Varadharajan et al. 2019) we detected haplotypes
 52 in three contexts. First, some haplotypes were originally assembled as
 53 separate contigs leading to false duplication of a region in the assembly.
 54 Second, haplotypes were assembled to the ends of subsequent contigs
 55 and occurred as duplicates on both sides of a contig gap. Third, hap-
 56 lotypic regions, exemplified by an inversion in LG19, were assembled

57 as mosaics of the two haplotypes. Using the novel features of Lep-
 58 Anchor, we could automatically remove a large proportion of the first
 59 two types of haplotypes while the correction of haplotypes of the last
 60 category was possible but demanded manual effort. Recognition and
 61 removal of haplotypes shortens the nine-spined stickleback reference
 62 genome and increases heterozygosity of the reference individual while
 63 the contig re-scaffolding enabled the identification of the centromere
 64 in all linkage groups. To demonstrate that this approach works for con-
 65 tig assemblies in general, we reassembled the latest published reference
 66 genome of the three-spined stickleback (*Gasterosteus aculeatus*; Peichel,
 67 Sullivan, Liachko, & White 2017) using one new linkage map and pub-
 68 licly available 10X Genomics linked read sequencing data (Berner et al.
 69 2019).

1 | MATERIALS AND METHODS

Nine-spined stickleback reference genome refinement

70 The starting point for this reference was the contig assembly and the
 71 genomic DNA sequence data from Varadharajan et al. (2019). In short,
 72

73

74 the ver. 6 genome by Varadharajan et al. (2019) was based on *de novo*
75 assembly of long PacBio reads, polishing with short reads and anchoring
76 with linkage maps. The contig assembly was refined in two places: (1) the
77 mitochondrial genome was reassembled from the short-read Illumina
78 data of the reference individual using the program MEGAHIT (ver. 1.2.9;
79 D. Li, Liu, Luo, Sadakane, & Lam 2015), and (2) a large inversion in LG19
80 was characterized and the region was reassembled using the combination
81 of programs Falcon Unzip (ver. 0.4.0; Chin et al. 2016), Trio Binning
82 (prerelease version; Koren et al. 2018), Canu (ver. 1.6; Koren et al. 2017)
83 and Pilon (ver. 1.22; Walker et al. 2014), all run with their default parameters.
84 The details of these steps are provided in the Supplementary methods.
85

86 A new ultra-high density linkage map was reconstructed based on
87 crosses of wild-caught marine nine-spined sticklebacks from Helsinki,
88 Finland ($60^{\circ}13'N$, $25^{\circ}11'E$). 99 F_1 -generation families were generated
89 at the University of Helsinki fish facility through artificial fertilizations
90 (Rastas, Calboli, Guo, Shikano, & Merilä 2016). Half-sib families were
91 formed by mating one female to two different males, thinning the families
92 to 25 offspring per family. The larvae were mass-reared in two large
93 aquaria and their family identity was later identified from the genotype
94 data. The parental fish were whole-genome sequenced (WGS; Illumina
95 HiSeq platforms, BGI Hong Kong) at 5–10x sequencing coverage and
96 the offspring were genotyped using the DarTseq technology (Diver-
97 sity Arrays Technology, Pty Ltd, Australia). The fastq files were mapped
98 to the contig assembly using BWA-MEM (ver. 0.7.15; H. Li 2013) and
99 SAMtools (ver. 1.9; H. Li et al. 2009). The genotype likelihoods were
100 called and the linkage mapping and the pedigree construction were con-
101 ducted using Lep-MAP3 (Rastas 2017). The details of the linkage map
102 reconstruction are provided in the Supplementary methods.

103 The resulting contig-assembly was anchored using Lep-Anchor (Ras-
104 tas 2020) following the standard pipeline (<https://sourceforge.net/p/lep-anchor/wiki/Home>) with default parameters (exception: minQual-
105 ity=1 for Map2Bed to assign more contigs into chromosomes). For the
106 anchoring, we (1) utilized three original linkage maps (Varadharajan et
107 al. 2019) and the newly reconstructed ultra-high density linkage map
108 concordant with the existing maps; (2) generated contig-contig align-
109 ments by running the two first steps of Haplomerger2 (Huang, Kang,
110 & Xu 2017); and (3) incorporated the raw PacBio reads by aligning
111 them to the contig assembly with minimap2 (ver. 2.17; H. Li 2018).
112 Full computer code for reproducing these analyses and instructions
113 for automated improvement of any reference genome assemblies are
114 available at https://github.com/mikkokivikoski/NSP_V7.

116 Contig classification and centromere annotation

117 In ver. 7, 1644 of the total 2487 contigs were not assigned to any of the
118 21 linkage groups (Table 1). We classified the contigs by analyzing their
119 sequencing depth (coverage) and repeat content. Illumina and PacBio
120 data (subreads) for the reference individual and for a pool of four female
121 individuals from the same Pyöreälampi pond (Illumina only, see Sup-
122 plementary methods for the details) were mapped and analyzed using

BWA-MEM and minimap2, respectively, and SAMtools. The coverage
123 analysis was carried out using Lep-Anchor's novel modules Coverage-
124 Analyser and CoverageHMM. Using CoverageAnalyser and a simple
125 mixture model, sequencing depth histogram was classified to (about)
126 zero, half, normal or high: Half and normal depths were modelled using
127 two normal distributions and the zero and high depth as a zeta distri-
128 bution (coverage + 1 \sim Zeta, the same distribution was used for both,
129 zero and high). Then CoverageHMM and a four-state hidden Markov
130 model (HMM) were used to classify each genomic position to four
131 states: zero, half, normal or high. The emission probabilities of the HMM
132 were taken from the mixture model (CoverageAnalyser) and maximum
133 likelihood transition probabilities along the physical (contig) coordi-
134 nates were learned using the Baum-Welch expectation-maximization
135 algorithm (Baum et al. 1972).

136 Repetitive regions were identified with RepeatMasker (ver. open-
137 4.0.5; Smit et al. 2013–2015 <http://www.repeatmasker.org>) by using the
138 species specific repeat libraries by Varadharajan (2019). Contigs with
139 >20% repeat content were classified as repetitive contigs (Fig. 1a). The
140 centromere-associated repeat sequence characterized by Varadharajan
141 (2019) was aligned against each unassigned contig with blastn (BLAST+
142 applications version 2.2.31+; Altschul, Gish, Miller, Myers, & Lipman
143 1990; Camacho et al. 2009). All contigs with at least one hit with e-value
144 < 10^{-5} were classified as putative centromeric contigs.

145 Alignments of centromere-associated repeat sequence were used
146 to determine the centromere positions (Suppl. Table 1, Suppl. Fig. 1).
147 Within each linkage group, Blast alignments with e-value < 10^{-5} were
148 assigned to three groups with k-mean clustering according to their pos-
149 ition. Clusters with less than 10% of the total number of hits were
150 discarded as outliers, and the centromeric region was defined to span
151 the remaining hits. Analyses were conducted and the results visualized
152 with R (ver. 3.4.4; R Core Team 2018 <https://www.R-project.org/>) using
153 packages ggplot2 (ver. 3.0.0; Wickham 2016) and ggforce (ver. 0.3.1;
154 Pedersen 2019 <https://CRAN.R-project.org/package=ggforce>).

156 Content of LG12 sex chromosome and LG19 inversion

157 Based on the female and male sequencing coverage, the sex-
158 chromosome part (1–25 Mpb) of the ver. 6 LG12 appeared to contain
159 contigs derived from X and Y chromosomes. We aimed to make LG12
160 haploid and purely X, and to identify differentiated Y-origin haplotypes
161 (Table 1). To investigate the new assembly of LG12 we joint-called
162 variable sites in a pool of the reference individual and four females
163 using GATK4 (ver. 4.0.1.2; McKenna et al. 2010), and defined a HMM
164 based on the frequency of homozygous reference and variant alleles in
165 females. We assumed that females are homozygous for the reference
166 allele in regions representing X and homozygous for the variant allele
167 in regions representing Y. The emitted statistic was $\frac{[0/0]}{[0/0]+[1/1]+1} \cdot 100$,
168 where [0/0] and [1/1] are the number of loci where an individual is
169 homozygous for reference or variant allele, respectively. The statistic
170 was calculated in 50 kb windows and rounded to the closest integer.
171 Low and high values of the statistic indicate X and Y chromosomes,

172 respectively, whereas values of around 50 indicate fine-scale mosaicism
173 of X and Y. The analysis was carried out in the sex-chromosome region
174 of the ver. 7 LG12 (1–16.9 Mbp) with R package HMM (ver. 1.0;
175 Scientific Software Development, Himmelmann 2010 <https://CRAN.R-project.org/package=HMM>).
176

177 The two alleles for the LG19 inversion were *de novo* assembled using
178 the long-read data from the reference individual and short-read data
179 from related individuals homozygous for the different copies (see Sup-
180 plementary methods for the details). Alternative versions of the genome
181 were created by inserting the newly assembled alleles into the reference
182 sequence. Individuals homozygous for the a and b alleles were mapped
183 to different versions of LG19 with BWA-MEM and SAMtools. Vari-
184 ants were called with bcftools mpileup (ver. 1.9; H. Li 2011) and single
185 nucleotide variants with quality score ≥ 5 were retained. Frequencies
186 of sites with homozygous and heterozygous variant alleles were calcu-
187 lated in 100 kb windows with Bedtools software (ver. 2.27.1; Quinlan &
188 Hall 2010).

189 Another HMM was defined to identify potential other inversion
190 haplotypes. We anticipated that a dense mosaic of haplotypes in the ref-
191 erence genome results in variation between homozygous reference and
192 variant alleles in an individual homozygous for one haplotype. There-
193 fore, the emitted statistic was defined as $-10 \log_{10} \left(\frac{([0/0] - [1/1])^2 + 1}{([0/0] + [1/1])^2 + 1} \right)$,
194 where [0/0] and [1/1] are the number of loci where an individual is
195 homozygous for reference or variant allele, respectively. The statistic
196 was estimated in 50kb windows and rounded to the closest integer; val-
197 ues above 40 were truncated to 40. Small values (e.g. high proportion
198 of both homozygous genotypes) indicated inversion region. The HMM
199 was applied to four female individuals and all 21 linkage groups.

200 Quality assessment with variant and synteny analyses

201 To compare the nine-spined ver. 6 and ver. 7 references, we called
202 autosomal SNPs of the reference individual (FIN-PYO-0). Reads were
203 mapped to both references using BWA-MEM and variants were called
204 with bcftools mpileup. SNPs were pruned with stringent criteria: SNPs
205 within repetitive or unmappable regions, within 20 bp of an indel,
206 of low quality (< 20) or with low (< 30) or high (> 70) depth were
207 discarded. Unmappable regions were determined using the approach
208 of Li (<http://lh3lh3.users.sourceforge.net/snpable.shtml>) and converted
209 to bed format using a script by Schiffels (<https://github.com/stschiff/msmc-tools>). SNPs found using ver. 6 were grouped into three cate-
210 gories: (1) found in autosomal linkage groups of ver. 7, (2) locus removed
211 from autosomal linkage groups of ver. 7, or (3) not called with ver. 7.
212 SNPs called using ver. 7 were grouped similarly but there were two addi-
213 tional groups for SNPs in regions where haplotype copy was removed
214 (Table 2).

215 The quality of ver. 6 and ver. 7 were also assessed by comparing
216 their synteny with the three-spined stickleback genome (Peichel et al.
217 2017). Based on the previously reported large-scale synteny to the
218 three-spined stickleback genome (Varadharajan et al. (2019); see also
219 Guo, Chain, Bornberg-Bauer, Leder, and Merilä (2013); Rastas et al.
220

221 (2016)), the homologous linkage groups of nine- and three-spined stick-
222 lebacks were aligned with minimap2 software. Previous studies (Rastas
223 et al. 2016; Shikano, Laine, Herczeg, Vilkki, & Merilä 2013) have shown
224 that LG12 is a fusion chromosome, and it was aligned against the three-
225 spined stickleback linkage groups 7 (1–14 Mbp) and 12. Alignment
226 fragments with less than 5000 matching base pairs were discarded and
227 the syntenies of the two assemblies with the three-spined stickleback
228 genome were compared by counting the number of changes in ori-
229 entation of consecutive fragments (Fig. 2b). BUSCO completeness of
230 ver. 6 was reported to be very high, containing 97.1% of tested genes as
231 complete BUSCOs (see Table 1 in Varadharajan et al. (2019)). Here, we
232 carried out the same analysis for both genome versions using BUSCO
233 ver. 5.0.0 (Seppey, Manni, & Zdobnov 2019). The command used
234 was 'docker run -u \$ID -v \$PATH:busco_wd ezelabgvabuso:v5.0.0_cv1
235 busco -m genome -i reference.fasta -o result_busco_reference -auto-
236 lineage-euk'. Contig classification, variant analysis, synteny comparisons
237 and other downstream analyses of the genome assembly, were exe-
238 cuted using Anduril 2 workflow platform (Cervera et al. 2019).

239 Three-spined stickleback reference genome refinement

240 We also tested the performance of Lep-Anchor with the three-spined
241 stickleback genome assembly (Peichel et al. 2017). First, a linkage map
242 was constructed with Lep-MAP3 based on the data set of 517 F₁-
243 offspring from 60 families (30 males, each crossed with two females)
244 described by Pritchard et al. (2017). The parents were wild caught
245 from the Baltic Sea and artificially crossed (see Leder et al. (2014) and
246 Pritchard et al. (2017) for more details). The linkage map reconstruc-
247 tion differed from that of the nine-spined stickleback in two places: the
248 pedigree was obtained from Pritchard et al. (2017) and, in Separate-
249 Chromosomes2, lodLimit was set to 25 to obtain 21 linkage groups.

250 The original scaffolded genome was partitioned into (about 16,000)
251 underlying contigs by cutting it at long runs of N's. An artificial map was
252 made to contain one marker per contig, listing contigs in the scaffold
253 order within each of the 21 linkage groups. To allow deviations from
254 the contig order of Peichel et al. (2017), the marker for the i:th contig
255 was given a map interval of [i, i+9]. Finally, an artificial alignment file
256 (paf format) was constructed with alignments for each adjacent con-
257 tig in the scaffolds. As for the nine-spined stickleback, we then run the
258 Lep-Anchor pipeline using the linkage map produced with Lep-MAP3
259 and the artificial map and alignment files. In the lack of long-read data,
260 we incorporated a scaffold level 10X Genomics genome assembly (Boot
261 Lake population, Vancouver Island, Canada; Berner et al. 2019) into the
262 input data. The 10X assembly and the three-spined stickleback contigs
263 were aligned with minimap2 and included as two copies to Lep-Anchor
264 to increase its weight in the optimisation score.

265 Lacking the short-read data for the reference individual, we called
266 SNPs for a male three-spined stickleback from Paxton Lake benthic
267 population, Canada (Samuk et al. 2017). The Illumina WGS data for
268 the sample SRR5626529 were downloaded from European Nucleotide

269 Archive (ENA) and mapped with BWA-MEM to the published three-
270 spined stickleback genome and to the genome assembled here. SNPs
271 were called with bcftools mpileup as in the nine-spined stickleback (see
272 above). As the mean sequencing coverage of the sample as 15x, only
273 SNPs with depth between 7 and 23 were retained.

274 RESULTS

275 We used Lep-Anchor software and information from linkage map
276 anchoring, pairwise contig alignment and long-read bridging to reassem-
277 ble the nine-spined stickleback genome. Linkage map anchoring allowed
278 assigning 274 previously unassigned contigs to the linkage groups (LGs)
279 and pairwise contig alignments revealed 10% of the previous assembly
280 as haplotypes (Fig. 1a). Of the 843 contigs in linkage groups, Lep-Anchor
281 could assess 763 to be scaffolded in correct orientation. Removal of
282 haplotypes and linking of adjacent contigs reduced the number of contig
283 gaps and more than doubled the N50 contig length as well as increased
284 the number single-copy BUSCO genes (Table 1). With a more accurate
285 representation of the haploid genome, the total length of the reference
286 decreased by 55 Mbp (Table 1). It is noticeable that, with the exception
287 of one linkage map produced here, these improvements were gained
288 with a more efficient use of data generated for the original assembly. In
289 addition to automated improvements with Lep-Anchor, we assembled
290 and incorporated the native mitochondrial genome and used additional
291 data from related individuals to characterize and reassemble a large
292 inversion in LG19.

293 The improved assembly brings noticeable gains, and we could now
294 successfully map the centromere associated repeat and unambigu-
295 ously identify the centromere positions in all linkage groups (previ-
296 ously missing from LG1 and LG16, and incoherent in LG10 and LG14,
297 Suppl. Fig. 2; see Varadharajan et al. (2019)). Removal of haplotypes and
298 other changes in the genome assembly affects read mapping and single
299 nucleotide variant calling. More even read depth and the anticipated
300 mean depth indicate that the reference has become more haploid and
301 contains fewer haplotype copies (Suppl. Fig. 3). In comparison to the
302 ver. 6, the heterozygosity of the reference individual increased by 14%
303 (Table 2), illustrating how the variation is concentrated in few regions
304 and how these variable regions then get assembled as separate haplo-
305 types. Indeed, most (78%) of the newly identified SNPs were in regions
306 where haplotype variants were removed from the reference and reads
307 from variant alleles now map to the same copy of the genomic region
308 (Fig. 1b-c, Table 2). New SNPs in other regions were a minority and their
309 allelic depth deviated from the expected (Suppl. Fig. 4).

310 Content of the LG12 changed considerably from ver. 6 to ver. 7 as
311 one of the homologous copies in X and Y chromosomes were removed
312 (Fig. 1a). As a result, the sex chromosome part of LG12 is close to a
313 haploid representation and few regions show zero read depth (Fig. 2a).
314 This also increases the heterozygosity of the male reference individual
315 (Fig. 2a), the newly identified SNPs arising from differences between X
316 and Y chromosomes, while no increase is observed in females (Fig. 2a).
317 Although homologous sequences are represented only once, the sex

318 chromosome is still a mosaic of X and Y chromosomes and females
319 show both homozygous variant and reference alleles (Fig. 2a). An HMM
320 analysis confirmed the mosaicism and indicated the sex chromosome
321 assembly to be 57% of X chromosome (Suppl. Fig. 5). Despite the
322 mosaicism, the reassembly improved the synteny of LG12 with the
323 three-spined stickleback counterparts (Fig. 2b).

324 Scaffolding with Lep-Anchor had a minor impact on the variant allele
325 frequencies in the LG19 inversion region (Fig. 3a). The reason for this is
326 that the original contigs were mosaics of the two alleles and an improved
327 ordering of contigs does not correct for their internal errors. The newly
328 assembled contigs and the scaffolded alleles for the LG19 block revealed
329 that there, indeed, are two segregating inversion haplotypes in the study
330 population, and that the reference individual (see methods) is heterozy-
331 gous (Fig. 3a). As expected, the variant allele frequencies across the
332 newly assembled haplotypes are either zero or twice as high as with
333 the original mosaic assembly for individuals homozygous for the two
334 alleles (Fig. 3a). Although the mosaicism had a large impact on variant
335 allele frequencies, its effect on SNP frequency was small. There are more
336 SNPs according to ver. 7 but most of them are found due to haplotype
337 removal and few of them are in the inversion region. With the HMM and
338 data from the four females, we found four observable large regions that
339 indicate fine-scale mosaic of two diverged haplotypes (Fig. 3b, see also
340 Suppl. Table 3.). All these four regions were identified in both genome
341 versions which suggests that the corresponding contigs are erroneously
342 assembled as in LG19.

343 Comparable data were not available for three-spined stickleback. We
344 constructed a contig assembly by partitioning the full-length sequence
345 (Peichel et al. 2017) at long runs of N's, and constructed a linkage map
346 for a distantly related population (Pritchard et al. 2017). In the absence
347 of long-read data, we bridged the contigs of the original assembly using
348 scaffolds of a 10X Genomics assembly (Berner et al. 2019). In this
349 reassembly, we identified 1,831 haplotype contigs, most of them unas-
350 signed, and were able to add 176 previously unassigned contigs to the
351 linkage groups. The ungapped length of the 21 linkage groups, repre-
352 senting the 21 chromosomes, decreased from 426 Mbp to 423 Mbp
353 and the ungapped length of the unassigned contigs decreased from 21
354 Mbp to 13 Mbp. N50 of the original and our new genome are 83,717
355 and 87,370 bp, respectively (Suppl. Table 2). With the new reference
356 we found 0.62% more autosomal SNPs in a sample from Paxton Lake,
357 Canada, than were found using the original assembly (Table 2). Although
358 the background heterozygosity of this individual was orders of mag-
359 nitude higher than in our nine-spined stickleback reference individual,
360 most of the newly identified SNPs (52%) were in regions where hap-
361 lotype variant was removed from the reference genome. Whereas the
362 median sequencing depth of the sample was 15x for both genome ver-
363 sions, the depth for the identified haplotype regions was 9x and 15x
364 in the published and new assembly, respectively, indicating successful
365 haplotype removal.

TABLE 1 Summary of the differences between the two nine-spined stickleback genome assemblies

Feature	ver. 6	ver. 7	%Change
N50 contig size (bp)	1,202,809	2,794,615	+132.34
Total length of the assembly (bp) [†]	521,233,387	466,582,808	-10.48
Total length of the 21 linkage groups (bp)	444,482,085	439,721,235	-1.08
LG12 length (bp)	40,899,740	33,585,825	-17.88
Contigs in linkage groups (contig chains) [‡]	686 (NA)	843 (362)	+22.89 (NA)
Contigs in LG12	244	150	-38.52
Contigs not assigned to linkage groups (length)	4,616 (76,734,720 bp)	1,644 (27,251,636 bp)	-64.38 (-64.49)
Contigs not in linkage groups of other assembly (LG12)	117 (109)	274 (15)	
Contigs with known orientation	Not assessed in ver. 6	763 (427,086,963 bp)	
Complete BUSCOs	3572 (98.2%)	3573 (98.2%)	+0.03
Complete single-copy BUSCOs	3438 (94.5%)	3529 (97.0%)	+2.65
Complete duplicated BUSCOs	134 (3.7%)	44 (1.2%)	-67.16
Fragmented BUSCOs	18 (0.5%)	16 (0.4%)	-11.11
Missing BUSCOs [§]	50 (1.3%)	51 (1.4%)	+2.00
Total BUSCO groups searched	3640	3640	0

[†] Includes 21 linkage groups with gaps, unassigned contigs and mitochondrial sequence.

[‡] Contig chain refers to group of contigs joined without gap in ver. 7. In ver. 6, all contigs had a gap in between.

[§] See Suppl. Table 3

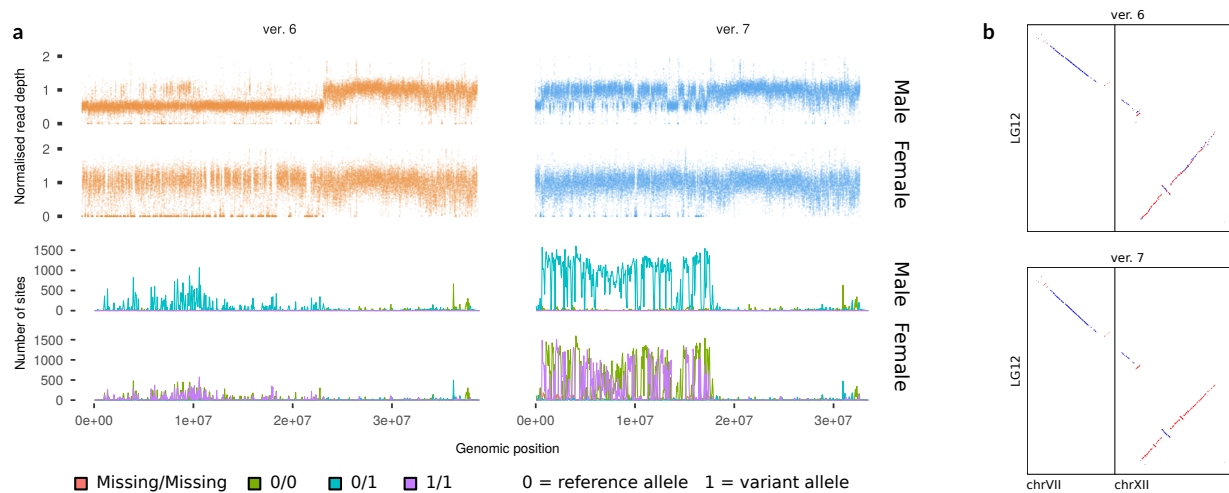


FIGURE 2 Improvements in LG12 sex chromosome. (a) Normalised read depth (top) of the male reference individual (50x coverage) and a female (10x, FIN-PYO-20) is closer to the expected (one) in ver. 7 (right) and fewer regions show zero depth. Ver. 7 has more segregating sites (bottom) and especially sites where the reference individual is heterozygous (turquoise) and the female is homozygous (green, purple). Number of sites is calculated in 100 kb windows. (b) The synteny of the nine-spined stickleback LG12 with the three-spined stickleback genome (x axis) is more contiguous in ver. 7, and there are fewer changes in contig order. Red and blue colors indicate forward and reverse alignments, respectively.

366 DISCUSSION

367 Reconstructing a linear reference genome is a challenging, yet an instru-
 368 mental task. Interpretation of genomic data is often made with the
 369 assumption that the reference genome is a complete haploid repre-
 370 sentation of the actual genome. The errors in the genome directly
 371 affect the conclusions drawn, and for instance, missing SNPs influence
 372 the site frequency spectrum that is essential in demographic analyses
 373 (Han, Sinsheimer, & Novembre 2014). More directly, presence of hap-
 374 lotype copies in a reference genome can make a highly diverged region

375 seem exceptionally conserved and can thus seriously mislead variation-
 376 based functional analyses. Given the severe consequences of the errors,
 377 efforts to improve reference genomes are needed, and here we have
 378 described an approach to make reference genomes more haploid and
 379 more contiguous using the Lep-Anchor software (Rastas 2020).

380 Faced with the dilemma of correctly separating duplicated genome
 381 regions while simultaneously collapsing and merging haplotypic differ-
 382 ences into a haploid sequence, all assembly programs are poised to make
 383 errors. The magnitude of these errors depends on the heterozygosity of

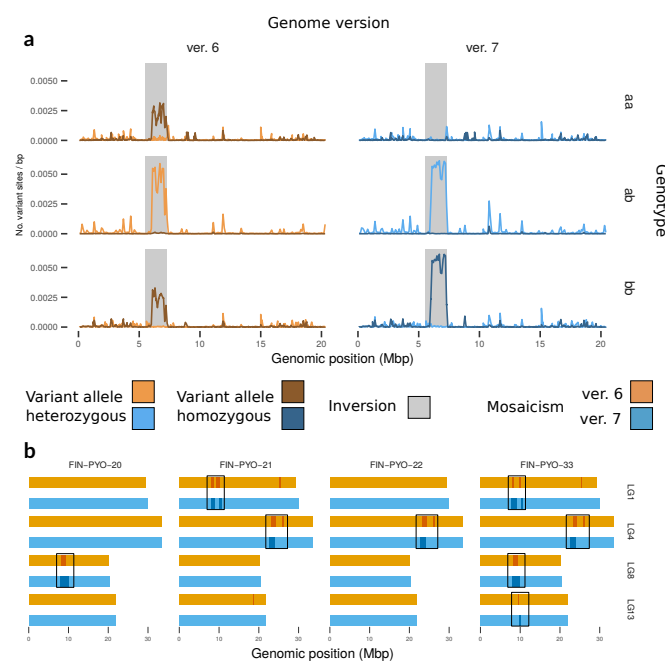


FIGURE 3 Examples of finescale mosaicism in the nine-spined stickleback reference genome. (a) When mapped to ver. 6, individuals homozygote for the LG19 inversion haplotypes (aa and bb; top and bottom) show high frequency of variant alleles in the inversion region. In ver. 7 with the reassembled inversion haplotype, individuals homozygous for the reference haplotype (top) have no variant alleles whereas those homozygous for the alternative allele (bottom) show two-fold frequency across the region. (b) Using a HMM, four candidates of finescale mosaicism (dark bands) similar to the LG19 inversion were identified. Here, the Viterbi path of the HMM algorithm is shown and only regions detected in both genome versions are highlighted with rectangles (see Suppl. Table 4 and Suppl. Fig. 6 for the genomic coordinates and posterior likelihoods).

384 the reference individual and on the type of input data, long reads spanning
 385 more distant sites and thus capable of creating longer haplotype

TABLE 2 Number of autosomal SNPs of detected by mapping short read data against the published and the new assemblies. SNPs may be missing because the region is involved in haplotype removal or is excluded from the autosomes. “Unknown” indicates SNPs identified in regions with no contig changes or removed haplotypes.

Version found	Reason not in other	Nine-spined	Three-spined
Both	–	23,576	2,278,066
Published only	Not in autosome	11	3,672
	Unknown	88	1,792
New only	Haplotype removed	2,110	6,912
	Haplotype trimmed	514	3,217
	Not in autosome	248	5,160
	Unknown	500	4,342

blocks, while the direction of the bias to either too long or too short genome depends on the algorithm. While the three-spined stickleback genome is based on relatively old data and is established over years of refinement, the nine-spined stickleback genome is an example of a modern reference genome built using the best practices. We demonstrated our method’s potential by showing how the latter, an already very high quality reference genome, could be greatly improved by more efficient use of the original sequencing and mapping data (Fig. 1, Table 1). Improvements were based on linking, reassembly and improved scaffolding of the contigs with joint use of linkage map anchoring and long read sequencing data, as well as characterization and removal of alternative haplotypes. The improvements on the three-spined stickleback genome were more modest but we could still both add new contigs into the linkage groups and remove haplotype copies (Suppl. Table 2, Suppl. Fig. 7), resulting in an 0.62% increase in number of segregating sites in a sample from the Paxton Lake benthic population (Table 2). We anticipate that the more modest changes in comparison to the nine-spined were due to absence of long reads and lower number of linkage map markers per contig in the three-spined data: 4.2 and 1.7 markers on average per contig in the nine and three-spined stickleback, respectively. While the three-spined stickleback analyses demonstrate that Lep-Anchor can improve even highly polished assemblies, they also illustrate how various data types, for example contigs from the 10X Genomics platform, can be incorporated in genome refinement.

In the nine-spined stickleback, most of the removed haplotypes were among the unassigned contigs and only one contig was moved between two linkage groups (Fig. 1a), underlining the high quality of the original scaffold. Although we were not able to place all contigs in the linkage groups, we were able to divide them in putative classes based on the read depth and their repeat content, those with high repeat content (either centromere or other) forming the largest groups of unassigned contigs. Although repetitive regions are difficult to assemble and scaffold using the type of data available, we were able to improve the centromeric regions (Fig. 1b) and our approach can be useful for repetitive regions more generally. Some unassigned contigs had low or even zero read depth, but as we did not detect any obvious contamination when aligning them to the NCBI database, those were retained in the reference genome.

Removal of haplotypes lead to identification of ca. 14% more autosomal SNPs in the nine-spined stickleback reference individual (Table 2). Finding more SNPs *per se* is not evidence for better assembly, and removal of true paralogous regions could lead to incorrect increase in SNP numbers. However, together with more uniform sequencing depth (Suppl. Fig. 3), strong evidence of successfully identified haplotypes (Fig. 1b-c) and higher number of single-copy BUSCOs (and lower number of duplicated BUSCOs, Table 1), our results show that genetic variability can be underestimated if the reference genome contains haplotypes. One should note, though, that our reference comes from a very small population and has extremely low background heterozygosity. Haplotypes, by definition, require variation between the copies and in our reference individual an exceptionally large proportion of the

437 variation is concentrated within a small number of regions. The three-
438 spined stickleback individual studied here had two orders of magnitude
439 higher heterozygosity and, although the absolute numbers were larger,
440 the relative impact of the reassembly on the SNP numbers was much
441 smaller (Table 2). The minority of newly identified SNPs that were not
442 within haplotype regions (22% of the novel SNPs in the nine-spined
443 stickleback) may have emerged because of short similarities between
444 contigs that were not classified as haplotypes. They may also be related
445 to changes in mapping of the read pairs in regions where haplotype
446 copies have been removed or contig orientation or order has changed.
447 Nonetheless, the evidence for some of those SNPs is questionable as
448 their allelic depth deviates from the expected (i.e. 0.5; Suppl. Fig. 4) and
449 one may want to filter them from downstream analyses.

450 Nine-spined stickleback LG12 is formed by fusion of chromosomal
451 segments that correspond to chromosomes 7 and 12 of the three-
452 spined stickleback (Fig. 2b; Shikano et al. 2013). This rearrangement has
453 occurred after the split of the three-spined and the nine-spined stick-
454 lebacks 17 million years ago (Guo et al. 2019) but the exact timing is
455 unclear (Shikano et al. 2013). While 15 Mbp in one end of LG12 behaves
456 like an autosomal chromosome, the 17 Mbp (25 Mbp in ver. 6) in the
457 other end contains the sex-determination region and behaves like a sex
458 chromosome (Fig. 2a). While parts of the sex-chromosome region seem
459 very similar, other parts have differentiated significantly, and assembling
460 complete X and Y chromosomes based on a single male reference indi-
461 vidual is extremely challenging. Although our HMM analysis indicated
462 that the LG12 assembled here is only 57% of X (Suppl. Fig. 5), we are
463 confident that the sequence content of the current version is close to
464 haploid presentation of X and the error is mainly in the SNP polariza-
465 tion. This is supported by the improved synteny with the three-spined
466 stickleback genome (Fig. 2b) but especially by the more uniform read
467 depth and more constant nucleotide diversity across the whole LG12 in
468 females (Fig. 2a). The original sequencing data for the nine-spined stick-
469 leback reference are slightly outdated by modern standards, and we did
470 not attempt to scaffold both X and Y copies of LG12. Fully separating
471 the two should be relatively straightforward by obtaining long-read or
472 linked-read data for both sexes with the latest sequencing technology.

473 Without genotype phasing, a haploid reference genome is a mosaic
474 of maternal and paternal haplotypes and the reference alleles are drawn
475 randomly. If parental haplotypes are clearly different, they are assem-
476 bled as separate copies and appear as duplicates in the contig assem-
477 bly; if the differences are punctuated by local similarities, the haploid
478 consensus may alternate between the two parental haplotypes. It is
479 evident that if the underlying contigs are erroneously assembled, their
480 re-ordering cannot make the reference perfect. In the nine-spined stick-
481 leback, the inversion in LG19 and the sex-chromosome region LG12
482 demonstrate how diverged haplotypes complicate the assembly of a
483 haploid reference genome. On the other hand, the characterization
484 of the inversion haplotypes provides an example of how TrioBinning
485 (Koren et al. 2018) can be utilized without a trio and long-read sequenc-
486 ing data combined with population level whole-genome sequencing
487 data allow assembling the segregating haplotypes. We acknowledge

488 that our HMM for identifying regions of diverged haplotypes provides
489 only indicative results (Fig. 3b) but it does suggest that haplotypes
490 can be fairly common in the nine-spined stickleback which is in line
491 with findings regarding other fish (Stemple 2013) and humans (Sudmant
492 et al. 2015). We also anticipate that highly concentrated alternation
493 between two homozygous genotypes is a usable statistic for explo-
494 ration and more sophisticated detection methods based on that could
495 be devised. Identification of such regions requires the studied individ-
496 ual to be heterozygous and therefore all regions were not supported by
497 all individuals. Having a single continuous haplotype, such as the inver-
498 sion in LG19, in the reference genome correctly phases the alternative
499 alleles (Fig. 3a) and allows studying the differences between the hap-
500 lotypes. However, representation of potential structural differences is
501 difficult and it is evident that methodological work to incorporate mul-
502 tiple haplotypes in a reference genome, e.g. using variation graph data
503 structures, is urgently needed (Paten, Novak, Eizenga, & Garrison 2017).

504 Haplod reference genomes based on a single individual, such as the
505 one here, represent only one version of the species' genome which
506 may cause reference bias and thus affect various downstream anal-
507 yses and the conclusions drawn from them (Ballouz, Dobin, & Gillis
508 2019; Paten et al. 2017). Although a linear reference does not represent
509 the full species diversity, they are widely used and provide a starting
510 point for analysis of genomic variation between individuals and pop-
511 ulations. In the future, pan-genome representations and graph-based
512 algorithms will likely change the way reference genomes are repre-
513 sented and analyzed (Paten et al. 2017; Sherman & Salzberg 2020).
514 Since linear genomes are still widely used, their improvements are rel-
515 evant and our work demonstrates that significant enhancements can
516 be obtained with efficient use of the existing data. Moreover, char-
517 acterization of haplotypes is instrumental in more inclusive genome
518 representations, increasing the relevance of our approach.

DATA AVAILABILITY

519 Sequence data that support the findings of this study have been
520 deposited in European Nucleotide Archive (ENA) under the acces-
521 sions PRJEB39736 (linkage map parents), PRJEB39760 (linkage
522 map offspring), PRJEB33474 and PRJEB39599 (whole-genome
523 sequenced individuals from Pyöreälampi and Kirkasvetinen). Link-
524 age maps and genomes of the nine- and three-spined sticklebacks
525 are available at https://github.com/mikkokivikoski/NSP_V7 and in
526 ENA under the accession GCA_902500615. Computer code and
527 instructions for automated improvement of reference genome assem-
528 blies and scripts for reproducing these analyses are available at
529 https://github.com/mikkokivikoski/NSP_V7.

COMPETING INTEREST STATEMENT

531 The authors declare no competing interests.

488

489

490

491

492

493

494

495

496

497

498

499

500

501

502

503

504

505

506

507

508

509

510

511

512

513

514

515

516

517

518

519

520

521

522

523

524

525

526

527

528

529

530

531

532

ACKNOWLEDGEMENTS

We thank Chris Eberlein, Sami Karja, Takahito Shikano, and everyone else who helped in catching and rearing the fish utilized in this work. Thanks are also due to those who helped in DNA extractions, Laura Hänninen, Kirs Kähkönen, Miinastiina Issakainen and Sami Karja in particular. We thank Antoine Fraimout for help with relatedness analysis. Our research was supported by LUOVA doctoral programme of the University of Helsinki (funding to MK), Academy of Finland (# 129662, 134728 and 218343 to JM; # 322681 to AL), and grant from Helsinki Institute for Life Sciences (HiLife; to JM). We also wish to acknowledge CSC – IT Center for Science, Finland, for computational resources.

AUTHOR CONTRIBUTIONS

J.M. directed and organized the data collection. P.R. generated linkage maps and assembled reference genomes. M.K., A.L. and P.R. carried out the data analysis and interpretation of the results. M.K. was responsible for structuring and compiling the manuscript. The manuscript was written and edited by all authors.

References

Altschul, S. F., Gish, W., Miller, W., Myers, E. W., & Lipman, D. J. (1990). Basic local alignment search tool. *J. Mol. Biol.*, 215(3), 403–410.

Baker, M. (2012). *De novo* genome assembly: What every biologist should know. *Nat. Methods*, 9(4), 333–337.

Ballouz, S., Dobin, A., & Gillis, J. A. (2019). Is it time to change the reference genome? *Genome Biol.*, 20(1), 1–9.

Baum, L. E., et al. (1972). An inequality and associated maximization technique in statistical estimation for probabilistic functions of markov processes. *Inequalities*, 3(1), 1–8.

Berner, D., Roesti, M., Bilobram, S., Chan, S. K., Kirk, H., Pandoh, P., ... DeFaveri, J. (2019). *De Novo* sequencing, assembly, and annotation of four threespine stickleback genomes based on microfluidic partitioned DNA libraries. *Genes*, 10(6), 426.

Camacho, C., Coulouris, G., Avagyan, V., Ma, N., Papadopoulos, J., Bealer, K., & Madden, T. L. (2009). Blast+: architecture and applications. *BMC Bioinformatics*, 10(1), 421.

Ceballos, F. C., Joshi, P. K., Clark, D. W., Ramsay, M., & Wilson, J. F. (2018). Runs of homozygosity: windows into population history and trait architecture. *Nat. Rev. Genet.*, 19(4), 220–234.

Cervera, A., Rantanen, V., Ovaska, K., Laakso, M., Nuñez-Fontarnau, J., Alkodsi, A., ... Hautaniemi, S. (2019). Anduril 2: upgraded large-scale data integration framework. *Bioinformatics*, 35(19), 3815–3817.

Chin, C.-S., Peluso, P., Sedlazeck, F. J., Nattestad, M., Concepcion, G. T., Clum, A., ... Schatz, M. C. (2016). Phased diploid genome assembly with single-molecule real-time sequencing. *Nat. Methods*, 13(12), 1050–1054.

Church, D. M., Schneider, V. A., Graves, T., Auger, K., Cunningham, F., Bouk, N., ... Hubbard, T. (2011). Modernizing reference genome assemblies. *PLoS Biol.*, 9(7), e1001091.

Guo, B., Chain, F. J. J., Bornberg-Bauer, E., Leder, E. H., & Merilä, J. (2013). Genomic divergence between nine- and three-spined sticklebacks. *BMC Genomics*, 14(1), 756.

Guo, B., Fang, B., Shikano, T., Momigliano, P., Wang, C., Kravchenko, A., & Merilä, J. (2019). A phylogenomic perspective on diversity, hybridization and evolutionary affinities in the stickleback genus *Pungitius*. *Mol. Ecol.*, 28(17), 4046–4064.

Han, E., Sinsheimer, J. S., & Novembre, J. (2014). Characterizing bias in population genetic inferences from low-coverage sequencing data. *Mol. Biol. Evol.*, 31(3), 723–735.

Howe, K., Clark, M. D., Torroja, C. F., Torrance, J., Berthelot, C., Muffato, M., ... Stemple, D. L. (2013). The zebrafish reference genome sequence and its relationship to the human genome. *Nature*, 496(7446), 498–503.

Huang, S., Kang, M., & Xu, A. (2017). Haplomerger2: rebuilding both haploid sub-assemblies from high-heterozygosity diploid genome assembly. *Bioinformatics*, 33(16), 2577–2579.

Kong, A., Frigge, M. L., Masson, G., Besenbacher, S., Sulem, P., Magnusson, G., ... Stefansson, K. (2012). Rate of *de novo* mutations and the importance of father's age to disease risk. *Nature*, 488(7412), 471–475.

Koren, S., Rhie, A., Walenz, B. P., Dilthey, A. T., Bickhart, D. M., Kingan, S. B., ... Phillippy, A. M. (2018). *De novo* assembly of haplotype-resolved genomes with trio binning. *Nat. Biotechnol.*, 36(12), 1174–1182.

Koren, S., Walenz, B. P., Berlin, K., Miller, J. R., Bergman, N. H., & Phillippy, A. M. (2017). Canu: scalable and accurate long-read assembly via adaptive k-mer weighting and repeat separation. *Genome Res.*, 27(5), 722–736.

Korneliussen, T. S., Albrechtsen, A., & Nielsen, R. (2014). ANGSD: analysis of next generation sequencing data. *BMC Bioinformatics*, 15(1), 356.

Leder, E. H., McCairns, R. S., Leinonen, T., Cano, J. M., Viitaniemi, H. M., Nikinmaa, M., ... Merilä, J. (2014). The evolution and adaptive potential of transcriptional variation in sticklebacks—signatures of selection and widespread heritability. *Mol. Biol. Evol.*, 32(3), 674–689.

Li, D., Liu, C.-M., Luo, R., Sadakane, K., & Lam, T.-W. (2015). MEGAHIT: an ultra-fast single-node solution for large and complex metagenomics assembly via succinct de Bruijn graph. *Bioinformatics*, 31(10), 1674–1676.

Li, H. (2011). A statistical framework for SNP calling, mutation discovery, association mapping and population genetic parameter estimation from sequencing data. *Bioinformatics*, 27(21), 2987–2993.

Li, H. (2013). Aligning sequence reads, clone sequences and assembly contigs with BWA-MEM. Preprint at <http://arxiv.org/abs/1303.3997>. (00), 1–3.

629 Li, H. (2018). Minimap2: pairwise alignment for nucleotide sequences. 680
Bioinformatics, 34(18), 3094–3100. 681

630 Li, H., Handsaker, B., Wysoker, A., Fennell, T., Ruan, J., Homer, N., ... 682
Durbin, R. (2009). The sequence alignment/map format and 683
SAMtools. *Bioinformatics*, 25(16), 2078–2079. 684

631 McKenna, A., Hanna, M., Banks, E., Sivachenko, A., Cibulskis, K., Kernytsky, 685
A., ... DePristo, M. A. (2010). The genome analysis toolkit: 686
a MapReduce framework for analyzing next-generation DNA 687
sequencing data. *Genome Res.*, 20(9), 1297–1303. 688

632 Meltz Steinberg, K., Schneider, V. A., Alkan, C., Montague, M. J., Warren, 689
W. C., Church, D. M., & Wilson, R. K. (2017). Building 690
and Improving Reference Genome Assemblies. *Proc. IEEE*, 105(3), 691
422–435. 692

633 Paten, B., Novak, A. M., Eizenga, J. M., & Garrison, E. (2017). Genome 693
graphs and the evolution of genome inference. *Genome Res.*, 694
27(5), 665–676. 695

634 Peichel, C. L., Sullivan, S. T., Liachko, I., & White, M. A. (2017). Improvement 696
of the threespine stickleback genome using a Hi-C-based 697
proximity-guided assembly. *J. Hered.*, 108(6), 693–700. 698

635 Pengelly, R. J., & Collins, A. (2019). Linkage disequilibrium maps to 699
guide contig ordering for genome assembly. *Bioinformatics*, 35(4), 700
541–545. 701

636 Pritchard, V. L., Viitaniemi, H. M., McCairns, R. J. S., Merilä, J., Nikinmaa, 702
M., Primmer, C. R., & Leder, E. H. (2017). Regulatory architecture 703
of gene expression variation in the threespine stickleback 704
Gasterosteus aculeatus. *G3: Genes Genom. Genet.*, 7(1), 165–178. 705

637 Quinlan, A. R., & Hall, I. M. (2010). BEDTools: a flexible suite of utilities 706
for comparing genomic features. *Bioinformatics*, 26(6), 841–842. 707

638 Rastas, P. (2017). Lep-MAP3: robust linkage mapping even for low- 708
coverage whole genome sequencing data. *Bioinformatics*, 33(23), 709
3726–3732. 710

639 Rastas, P. (2020). Lep-Anchor: automated construction of linkage map 711
anchored haploid genomes. *Bioinformatics*, 36(8), 2359–2364. 712

640 Rastas, P., Calboli, F. C. F., Guo, B., Shikano, T., & Merilä, J. (2016). Con- 713
struction of ultradense linkage maps with Lep-MAP2: stickleback 714
F₂ recombinant crosses as an example. *Genome Biol. Evol.*, 8(1), 715
78–93. 716

641 Rice, E. S., & Green, R. E. (2019). New approaches for genome assembly 717
and scaffolding. *Annu. Rev. Anim. Biosci.*, 7(1), 17–40. 718

642 Roux, C., Fraïsse, C., Romiguier, J., Anciaux, Y., Galtier, N., & Bierne, N. 719
(2016). Shedding light on the grey zone of speciation along a 720
continuum of genomic divergence. *PLoS Biol.*, 14(12), 1–22. 721

643 Samuk, K., Owens, G. L., Delmore, K. E., Miller, S. E., Rennison, D. J., & 722
Schluter, D. (2017). Gene flow and selection interact to promote 723
adaptive divergence in regions of low recombination. *Mol. Ecol.*, 724
26(17), 4378–4390. 725

644 Schneider, V. A., Graves-Lindsay, T., Howe, K., Bouk, N., Chen, H.-C., 726
Kitts, P. A., ... Church, D. M. (2017). Evaluation of GRCh38 and 727
de novo haploid genome assemblies demonstrates the enduring 728
quality of the reference assembly. *Genome Res.*, 27(5), 849–864. 729

645 Schraiber, J. G., & Akey, J. M. (2015). Methods and models for 730
unravelling human evolutionary history. *Nat. Rev. Genet.*, 16(12), 727–740. 731

646 Seppey, M., Manni, M., & Zdobnov, E. M. (2019). BUSCO: Assessing 732
genome assembly and annotation completeness. In *Methods in 733
molecular biology* (pp. 227–245). Springer New York. Retrieved 734
from https://doi.org/10.1007/978-1-4939-9173-0_14 doi: 735
10.1007/978-1-4939-9173-0_14 736

647 Sherman, R. M., & Salzberg, S. L. (2020). Pan-genomics in the human 737
genome era. *Nat. Rev. Genet.*, 21(4), 243–254. 738

648 Shikano, T., Laine, V. N., Herczeg, G., Vilkki, J., & Merilä, J. (2013). 739
Genetic architecture of parallel pelvic reduction in ninespine 740
sticklebacks. *G3: Genes Genom. Genet.*, 3(10), 1833–1842. 741

649 Stemple, D. L. (2013). So, you want to sequence a genome... *Genome 742
Biol.*, 14(7), 128. 743

650 Sudmant, P. H., Rausch, T., Gardner, E. J., Handsaker, R. E., Abyzov, A., 744
Huddleston, J., ... Consortium, T. . G. P. (2015). An integrated 745
map of structural variation in 2,504 human genomes. *Nature*, 746
526(7571), 75–81. 747

651 Varadharajan, S. (2019). Ninespine_repeatlibrary.fasta. figshare. 748
doi: 10.6084/m9.figshare.10565792.v1 749

652 Varadharajan, S., Rastas, P., Löytynoja, A., Matschiner, M., Calboli, 750
F. C. F., Guo, B., ... Merilä, J. (2019). A high-quality assembly of 751
the nine-spined stickleback (*Pungitius pungitius*) Genome. *Genome 752
Biol. Evol.*, 11(11), 3291–3308. 753

653 Walker, B. J., Abeel, T., Shea, T., Priest, M., Abouelliel, A., Sakthikumar, S., 754
... Earl, A. M. (2014). Pilon: an integrated tool for comprehensive 755
microbial variant detection and genome assembly improvement. 756
PLoS ONE, 9(11), e112963. 757

654 Wickham, H. (2016). *ggplot2: Elegant graphics for data analysis*. Springer- 758
Verlag New York. 759

655

656

657

658

659

660

661

662

663

664

665

666

667

668

669

670

671

672

673

674

675

676

677

678

679